Mater. Res. Soc. Symp. Proc. Vol. 907E © 2006 Materials Research Society 0907-MM04-01.1

In-situ TEM studies of magnetization reversal processes in magnetic nanostructures

Amanda K Petford-Long[1], Thomas Bromwich[2], Amit Kohn[2], Victoria Jackson[2], Takeshi Kasama[3], Rafal Dunin-Borkowski[3] and Caroline A Ross[4]
[1]Argonne National Laboratory, 9700 S Cass Ave, Argonne, IL 60439.
[2]Dept. of Materials, Univ. of Oxford, Parks Road, Oxford OX1 3PH, UK.
[3]Dept. of Materials Science and Metallurgy, Univ. of Cambridge, Pembroke St, Cambridge CB2 3QZ, UK
[4]Materials Science and Engineering Dept, Massachusetts Institute of Technology, Cambridge, MA

ABSTRACT

One of the most widely studied types of magnetic nanostructure is that used in devices based on the giant magnetoresistance (GMR) or tunnel magnetoresistance (TMR) phenomena. In order to understand the behaviour of these materials it is important to be able to follow their magnetization reversal mechanism, and one of the techniques enabling micromagnetic studies at the sub-micron scale is transmission electron microscopy. Two techniques can be used: Lorentz transmission electron microscopy and off-axis electron holography, both of which allow the magnetic domain structure of a ferromagnetic material to be investigated dynamically in real-time with a resolution of a few nanometres. These techniques have been used in combination with *in situ* magnetizing experiments, to carry out qualitative and quantitative studies of magnetization reversal in a range of materials including spin-tunnel junctions, patterned thin film elements and magnetic antidot arrays. Quantitative analysis of the Lorentz TEM data has been carried out using the transport of intensity equation (TIE) approach.

INTRODUCTION

Over the past few years there has been an increased effort in the development of new materials for information storage applications, often in the form of layered structures containing many thin layers. This has been motivated by an intensive demand for improvement in information storage and memory density, mainly for graphics-intensive applications. The structures that are being most widely developed for read-heads rely on the giant magnetoresistance (GMR) or tunnel magnetoresistance (TMR) effect seen as a large change in resistance in an applied magnetic field [1]. Devices that make use of the GMR effect are spin-valve (SV) structures [2], and magnetic tunnel junctions (MTJs) [3]. The limits on memory density that can be achieved using solid state memory, in addition to the requirement for low power consumption and thus for non-volatile memory means that there has also been interest in the development of magnetic memory based on the GMR and TMR effects, namely magnetoresistive random access memory (MRAM) [4]. The GMR effect results from a change in the relative orientation of the magnetization in ferromagnetic (FM) layers separated by a non-magnetic spacer: parallel magnetization in adjacent layers gives a low resistance, whereas a high resistance is measured if the magnetization in adjacent layers is antiparallel. In SV and MTJ

structures, the magnetization direction of one of the FM layers is fixed by an adjacent antiferromagnetic (AF) layer through exchange coupling. The magnetization direction of the other FM layer (sense layer) can be rotated by applying a low external magnetic field (a few Oe). MTJ structures differ from SV films only in that the non-magnetic spacer later is an insulator, and the current is passed normal to the layers, requiring the electrons to tunnel quantum-mechanically from one FM layer to the other [5]. Additionally, developments in magnetic recording are going towards the fabrication of patterned media in which each data bit is stored in a physically isolated magnetic dot or pillar [6].

One of the fundamental properties that need to be addressed in all of the structures described above is the magnetization reversal mechanism in the FM layers and how this is affected by the size and shape of the structures into which the material is patterned for device applications. In addition, for memory and media applications many structures must be patterned lithographically into close-packed arrays, and the interactions between adjacent structures in the arrays becomes very important. Although information about magnetization reversal mechanisms can be obtained using bulk measurement techniques such as magnetometry, it is also important to be able to image the behaviour of individual structures. This becomes harder to do as the structures become smaller. There are four main techniques that are appropriate: firstly, Kerr microscopy, which is limited in resolution for imaging purposes, but can be used to obtain local hysteresis loops from single nanometre-scale structures [7]. Secondly X-ray microscopy and photo-emission electron microscopy, which have a resolution of the order of 50 nm, are element specific, and can be used to follow magnetization reversal mechanisms on the nanosecond timescale, but only if the reversal process is reproducible over many cycles because the signal collected over a single magnetization reversal is very low [8]. In addition, the technique is surface sensitive, making it hard to analyse buried layers. Thirdly, transmission electron microscopy (TEM) techniques such as Lorentz TEM (LTEM) and off-axis electron holography, which currently have the highest spatial resolution available and can be used to obtain fully quantitative images of the magnetic structure but with a time resolution that is limited to milliseconds. And fourthly magnetic force microscopy in which a magnetic tip is scanned over the surface of a sample and the stray fields are mapped. The spatial resolution of this technique is limited to 20 nm and it is best applied to the analysis of hard magnetic materials for which there is no danger of the probe itself modifying the magnetic structure of the sample.

All of the above techniques are described in the book edited by Hopster and Oepen [9]. In this paper we will concentrate on the use of *in situ* TEM techniques to study the magnetic domain structure and magnetization reversal mechanisms, with examples to illustrate the techniques as applied to patterned magnetic nanostructures with potential applications in information storage.

EXPERIMENTAL DETAILS

The spin-valve and Co dot films discussed in this paper were grown by sputter deposition, and the pillars by electrodeposition: both techniques produce polycrystalline films. They are commonly used to produce thin magnetic films and layered structures because they are relatively simple and cheap to implement, but the fact that the films are polycrystalline makes their characterisation more complex than for single crystal films. Microstructural defects and

inhomogeneities introduced by the deposition technique and by subsequent patterning into small structures can have a major influence on the magnetization reversal behaviour of the structures.

Lorentz microscopy

When electrons are incident on a thin magnetic specimen, the interaction of the electrons passing through the specimen results in magnetic contrast [10], which can be explained whether the electrons are considered as waves or as particles. If the electrons are considered as particles, the effect of the magnetic induction in the specimen is to deflect them (as a result of the Lorentz force) through an angle β given by:

$$\beta = (e\,\lambda\,\boldsymbol{B}\,t\,)/\,h \tag{1}$$

Where e is the electronic charge, $\boldsymbol{B}$ is the magnetic induction in the specimen, λ is the electron wavelength, t is the specimen thickness, and h is Planck's constant. The deflection is thus proportional to the thickness-magnetization product. Note that: only components of the magnetic induction normal to the electron beam give rise to a deflection; the stray fields above and below the specimen also contribute to the image because Lorentz microscopy is a transmission technique; and the deflection direction is perpendicular to the magnetization direction within the domain being imaged. An alternative way to consider the interaction is as change in phase of the incident electron wave. The phase gradient $\nabla\phi$ of the specimen transmittance is given by:

$$\nabla\phi = \frac{2\pi e t\,(\mathbf{B}\times\mathbf{n})}{h} \tag{2}$$

Where **n** is a unit vector parallel to the electron beam. Substituting typical numerical values shows that magnetic films should normally be regarded as strong, albeit slowly varying, phase objects [11]. For example, the phase change involved in crossing a domain wall usually exceeds π rad. Note that equations (1) and (2) hold for specimens in which **B** is constant through the film thickness.

There are two methods by which the magnetic domain structure can be imaged: the Fresnel mode and the Foucault mode and for reviews of these methods the reader is referred to Chapter 4 in ref. [7]. For the data shown in this paper, LTEM was carried out using a JEOL 4000EX TEM fitted with a low-field objective lens (vertical field at the specimen <6 Oe).

Quantitative analysis of LTEM data, in order to extract both the direction and magnitude of the magnetic induction in the sample, can be carried out using the transport of intensity equation (TIE) approach [12]. For this analysis a series of three images is recorded: an in-focus image plus two Fresnel images recorded with equal defocus on either side of focus. The images must be aligned accurately relative to each other and maps of the phase change experienced by the electron beam can then be reconstructed. The TIE analyses presented in results section were obtained via phase reconstruction using the QPe software package (Iatia Ltd.), which is based on the Fourier-transform approach developed by Paganin and Nugent [13]. A qualitative representation of experimental Foucault images could be obtained by taking the derivative of the

phase data with respect to the direction in which the objective aperture was introduced for the Foucault image.

Maps of the magnetic induction in the sample, in a plane perpendicular to the electron beam, can also be obtained using the differential phase contrast (DPC) technique of Chapman et al [14], which uses a scanning transmission electron microscope (STEM). The specimen is scanned with a small electron probe and the signal is detected on a circular detector split into four quadrants. The component of magnetization in two perpendicular directions can be calculated from the difference between the signals on opposite quadrants of the detector. Similar magnetization maps to those obtained using STEM DPC can be obtained in a conventional TEM by digitally combining series of Foucault images taken with small increments of electron beam tilt in two orthogonal directions [15].

Off-axis electron holography

Electron holography is based on recording an interference pattern from which the amplitude and phase of an object can be reconstructed [16]. Magnetic thin films are strong phase objects and the phase shift of the electrons passing through the specimen is proportional to the magnetic flux enclosed by the electron paths.

For the off-axis electron holography technique a specimen is chosen that does not completely fill the image plane (for example a small magnetic element or the edge of an extended film) so that only part of the electron beam passes through the specimen. An electrostatic biprism is then used to recombine the specimen beam and the reference beam so that they interfere and form a hologram. This can be digitised and image-processing techniques can then be applied to reconstruct a quantitative image of the magnetic domain structure. For further details of this technique the reader is referred to Chapter 5 in Ref. [7]. The holography data presented in this paper were recorded using a Philips CM300-ST TEM fitted with an electron biprism and Lorentz lens, and reconstruction of the data was carried out using scripts written in the Semper image processing package [17].

In situ imaging of magnetization reversal processes

LTEM and electron holography can be made even more powerful if a magnetic field can be applied *in situ* to the specimen so that magnetization reversal processes can be imaged. This can be done either by using magnetizing coils built into the TEM specimen holder or by tilting the specimen into the vertical lens field (if a standard objective lens is used). Using magnetizing coils in the holder removes the potential problem of the specimen experiencing a vertical component of magnetic field as well as an in-plane component. However, this technique can result in the need for an extra set of correction coils in the microscope column to realign the electron beam, which will be deflected by the applied magnetic field. For the LTEM analysis a magnetizing holder was used, capable of applying a field of up to ±800 Oe in the plane of the sample. For the holography experiments a field was applied by tilting the sample into the vertical field of the objective lens and then returning the sample to the 0 tilt position and decreasing the field at the specimen to zero prior to recording the holograms.

RESULTS

A configuration that is frequently seen in lithographically-defined small magnetic structures is a magnetic vortex. The magnetization is in the plane of the film, and rotates around a central core in which the magnetization is normal to the plane. The vortex has a low magnetostatic energy and so is energetically favourable. Understanding the way in which such structures form in single layer elements is important as it then allows the influence of a spacer and second FM layer to be determined separately once a full MTJ structure is fabricated. The magnetization reversal process by which a vortex structure forms in a micron-sized lithographically-defined circular magnetic element of thickness 20 nm is shown in the plan-view Fresnel mode LTEM images in figure 1a). As the magnetic field applied *in situ* in the TEM is increased to +5 Oe, two half vortices form at the left- and right-hand edges of the element (visible as bright and dark points). The partial vortices are connected together across the element by a pair of 180 domain walls (visible as bright and dark curved lines) so that the element consists of three domains with magnetization lying horizontally across the element alternately from left-to-right or right-to-left. As the field is increased further to +10 Oe, so the two partial vortices collapse together to form a single vortex (visible as a bright dot towards the top of the element). Note that the chirality of the vortex can be determined from whether the vortex core is dark or bright. A relatively high applied field is required to remove a vortex completely from the magnetic element (in this case +60 Oe), and the field that needs to be applied to remove the vortex can vary considerably between elements (for both single layer and tunnel junction structure elements), leading to a wide switching field distribution, which is not ideal for MRAM elements [18].

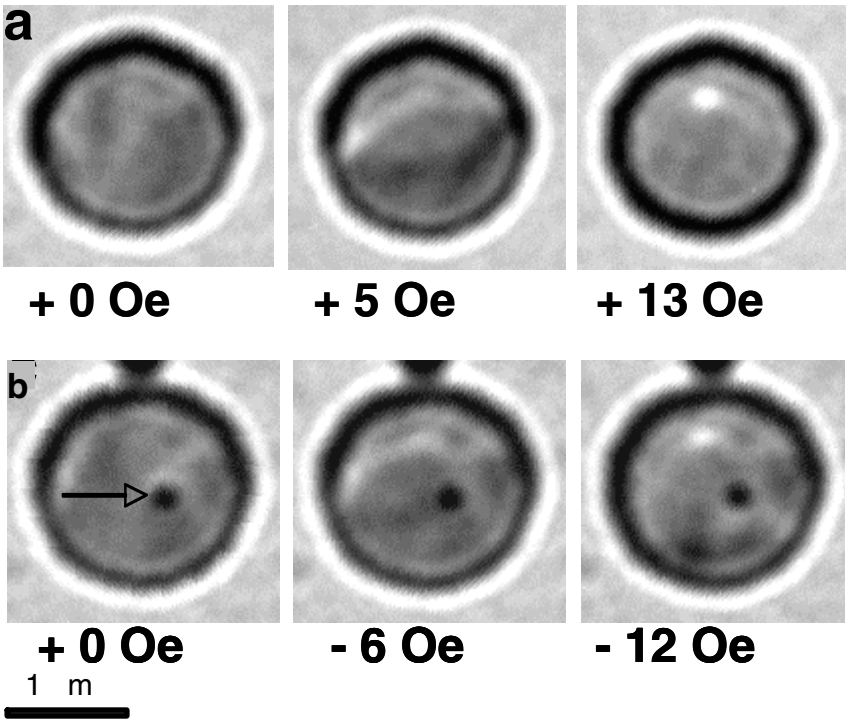

Figure 1 Fresnel mode LTEM images of 2 m diameter NiFe dot showing magnetization mechanism before a) and after b) introduction of induced defect (arrowed in b). Numbers indicate magnitude of magnetic field applied *in situ* in the TEM.

For comparison, figure 1b) shows the magnetization reversal process in the same element after a defect (arrowed) has been introduced by milling a small hole using a focused ion-beam system. As the *in situ* applied field is increased to −6 Oe so a similar domain structure forms as seen for the defect-free case, but the domain wall structure is more complex with some pinning at the induced defect. A further increase in applied field to −12 Oe results in the formation of two vortices as the domain walls unpin from the defect. The vortices have opposite chirality as can be seen from the fact that one has a bright core and the other a dark core. Note that the formation of a double magnetic vortex has so far not been reported in unpatterned circular magnetic elements but only in elements with a higher aspect ratio such as ellipses [19].

The Fresnel images seen in figure 1 provide a considerable amount of information about the magnetization reversal process, but the images are not quantitative. Figure 2 shows a comparison of micromagnetic modelling and quantitative LTEM data, obtained using the TIE analysis, for the NiFe element imaged in Figure 1a). Figure 2a) shows the results of micromagnetic simulations (carried out using the LLG software) and Figure 2b) shows maps of the in-plane magnetic induction with arrows indicating the direction of magnetization. These particular images are not fully quantitative because the defocus distance is too large for the TIE approach to enable the **B***t* product to be extracted, but they DO give a clear map of the magnetization directions in the structure. The images in the left-hand column show the magnetization state consisting of two partial vortices separated by two 180 walls running from left to right, and the right-hand column shows a magnetic vortex near the upper edge of the element.

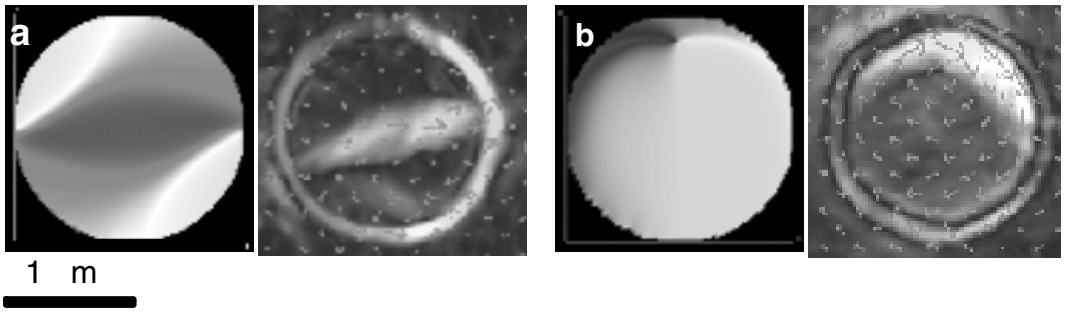

Figure 2 Micromagnetic simulation (left-hand image) and magnetization map reconstructed from LTEM data (right-hand image) for two different magnetic configurations of the NiFe element seen in Figure 1: a) multidomain state and b) magnetic vortex state.

As discussed earlier, off-axis electron holography and LTEM data are only sensitive to the magnetization in a plane normal to the electron beam. Analysis of samples with an out-of-plane magnetization direction therefore requires the sample either to be tilted in the electron beam or to be prepared in such a way that it can be viewed in cross-section. Figure 3 shows electron holography data from a row of Ni pillars (diameter 75 nm, height 175 nm), which has been cut from a two-dimensional array of pillars fabricated by interference lithography [20]. The interactions between adjacent pillars are of interest because of their potential application as patterned media. Figure 3 shows the array of pillars at remanence after application of two different applied fields inside the TEM: a) 247 Oe and b) 461 Oe). The arrows indicate the same pillar in the two images. The flux lines between the pillars indicate the stray fields that couple the pillars together: For the image shown in Figure 3a) the magnetization in the two pillars is in the

same direction and the flux links the top of one pillar to the bottom of the next. For the condition shown in Figure 3b), the middle pillar is oppositely magnetized to the other two and in this case the flux linkage is from top-to-top and bottom-to-bottom of adjacent pillars. The flux lines also indicate that the magnetization in the pillars does not lie directly along the pillar axis. Deviations from this arise because of the grain structure of the pillars, and indeed the internal magnetic structure in the pillars can be directly correlated with their grain structure. This arises because the local magnetocrystalline anisotropy influences the magnetization direction.

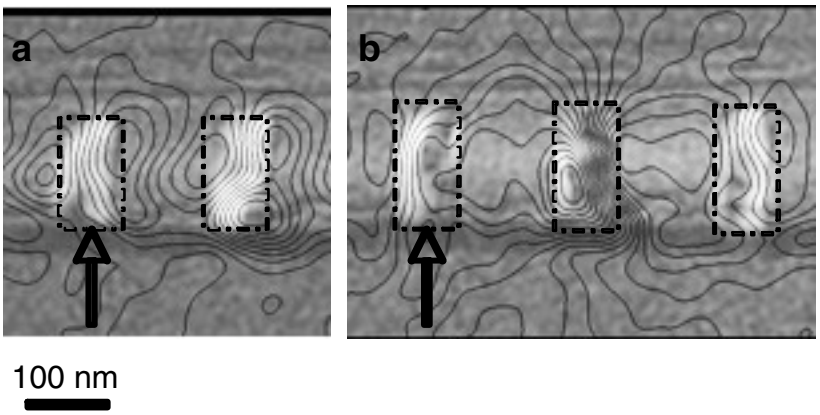

Figure 3 Magnetic phase images showing magnetic flux linking Ni pillars after application of in situ magnetic field of a) 247 Oe and b) 461 Oe. The dashed outlines indicate the positions of the pillars and the same pillar is arrowed in a) and b). Note the flux lines indicating coupling between the pillars. Phase contour spacing is 0.2 radians.

In situ LTEM experiments are not limited only to the application of an applied magnetic field. *In situ* heating of the structures while magnetizing has allowed the temperature dependence of parameters such as the pinning field of the antiferromagnet to be followed. This can be seen in Figure 4, which shows Fresnel mode LTEM images of the magnetization reversal process in a spin-valve as a function of temperature. At a temperature below the exchange blocking temperature of the antiferromagnet (100 C), the magnetization only reverses in the free ferromagnetic layer so that the final magnetization configuration is antiparallel alignment of the magnetization in the two FM layers. When the temperature is increased to 250 C the exchange pinning of the pinned FM layer to the antiferromagnetic layer is overcome, and the magnetization in both ferromagnetic layers reverses. This is clearly seen in the lower row of images, in which pairs of bright or dark lines can be seen at the domain wall positions. This contrast is only possible if one of the pair of walls is in each of the two ferromagnetic layers.

The examples given above indicate some of the possible ways in which *in situ* TEM experiments combining LTEM or electron holography with magnetizing can be used to follow the magnetization reversal mechanisms in thin film magnetic nanostructures. Of course these are not the only possibilities and it is often by combining capabilities that details of the reversal processes and their effect on device properties can be understood. For example, facilities that allow simultaneous application of a magnetic field and a current through a SV element have allowed the GMR curve to be correlated with the magnetization reversal process. This has

allowed the effect of parameters such as current value and direction on the magnetization reversal mechanism to be understood [21].

CONCLUSIONS

In summary, the use of electron microscopy has enabled a considerable amount of information about the microstructure, composition distribution, magnetization reversal mechanism and transport properties in SV and STJ structures to be determined. As the structures and devices become smaller and more complex, so the need to analyse them at high spatial resolution will continue to be of great importance.

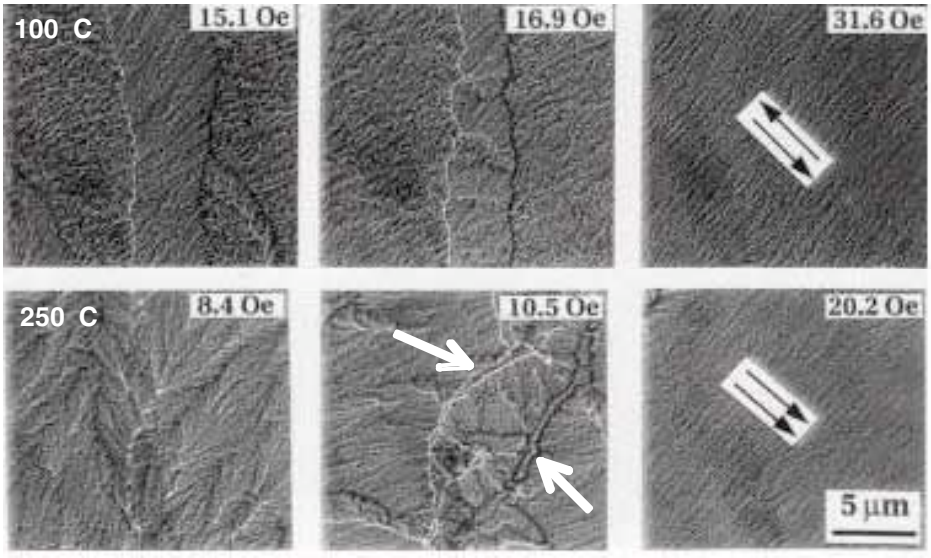

Figure 4 Fresnel mode LTEM plan-view images of the magnetization reversal in a spin-valve as a function of temperature. Initially the magnetization in the two FM layers is parallel and points towards the top left. At 100 C the magnetization in the free layer alone reverses, whereas at 250 C the magnetization in both the FM layers reverses, as indicated by the presence of pairs of light or dark walls (arrowed in lower middle image). The numbers on each image indicate the field applied *in situ* in the TEM.

ACKNOWLEDGEMENTS

The STJ and SV studies described above were carried out as part of a collaborative project with Hewlett-Packard Labs, Palo Alto. We thank Profs G W Smith and D J Fray for the provision of laboratory space. TJB acknowledges funding from the EPSRC; CAR and FC acknowledge the NSF for financial support; TK acknowledges financial support from The Institute of Physical and Chemical Research, Saitama. Japan and RED is grateful to the Royal Society for financial support.

REFERENCES

[1] M.N. Baibich, J.M. Broto, A. Fert, F. Nguyen Van Dau, F. Petroff, P. Etienne, G. Creuzet, A. Friedrich and A. Chazelas, Phys. Rev. Lett. **61,** 2472 (1988).
[2] B. Dieny, V.S. Speriosu, S.S.P. Parkin, B.A. Gurney, D.R. Wilhoit and D. Mauri, Phys. Rev. **B43**, 1297 (1991).
[3] W.J. Gallagher, S.S.P. Parkin, L. Yu, X.P. Bian, A. Marley R.A. Altman, S.A. Rishton, K.P. Roche, C. Jahnes, T.M. Shaw and X. Gang, J. Appl. Phys. **81,** 3741 (1997).
[4] S. Tehrani, J.M. Slaughter, M. Deherrera, B.N. Engel, N.D. Rizzo. J. Salter, M. Durlam, R.W. Dave, J. Janesky, B. Butcher, K. Smith and G. Grynkewich, Proc. IEEE **91(5),** 703 (2003).
[5] E.Yu Tsymbal, O.N. Mryasov and P.R. LeClair, J. Phys.: Condens. Matter **15**, R109 (2003).
[6] B.D. Terris and T. Thomson, J. Phys. D: Appl. Phys. **38,** R199 (2005).
[7] D.A. Allwood, G. Xiong, M.D. Cooke and R.P. Cowburn, J. Phys. D: Appl. Phys. **36**, 2175 (2003).
[8] P. Fischer, Curr. Opin. Sol. Stat. Mat. Sci. **7**, 173 (2003).
[9] *Magnetic Microscopy of Nanostructures* edited by H. Hopster and H.P. Oepen (Springer, Berlin, Heidelberg, 2005).
[10] M.E. Hale, H.W. Fuller and H. Rubenstein, J. Appl. Phys. **30**, 789 (1959).
[11] J.N. Chapman, J.Phys. D: Appl.Phys. **17**, 623 (1984).
[12] M. De Graef and Y. Zhu, J. Appl. Phys. **89**, 7177 (2001).
[13] D. Paganin and K.A. Nugent, Phys. Rev. Lett. **80**, 2586 (1998).
[14] J.N. Chapman and G.R. Morrison, J. Magn. Mag. Mat. **35**, 254 (1983).
[15] A.C. Daykin and A.K. Petford-Long, Ultramicrosc. **58**, 365 (1995).
[16] A. Tonomura, T. Matsuda, J. Endo, T. Arii and K. Mihama, Phys. Rev. Lett. **44**, 1430 (1980).
[17] W.O. Saxton, T.J. Pitt and M. Horner, Ultramicrosc. **4**, 343 (1979).
[18] Y.K. Lee, B.S. Chun, Y.K. Kim, I. Hwang, W. Park, T. Kim, H. Kim, J. Lee and W.C. Jeong, IEEE Trans. Mag. **41,** 883(2005).
[19] T. Okuno, K. Mibu and T. Shinjo, J. Appl. Phys. **95**, 3612 (2004).
[20] C.A. Ross, M. Hwang, M. Shima, J.Y. Cheng, M. Farhoud, T.A. Savas, Henry I. Smith, W. Schwarzacher, F.M. Ross, F.B. Humphrey and M. Redjdal, Phys. Rev. B **65** 144417 (2002).
[21] X. Portier, A.K. Petford-Long, T.C. Anthony and J.A. Brug, J. Magn. Magn. Mater. **187,** 145 (1998).